Enhanced Three-Phase Shunt Active Power Filter Interfacing a Renewable and an Energy Storage System

Ana Rodrigues
Centro ALGORITMI
University of Minho
Guimaraes, Portugal
arodrigues@dei.uminho.pt

Catia Oliveira
Centro ALGORITMI
University of Minho
Guimaraes, Portugal
c.oliveira@dei.uminho.pt

Tiago J. C. Sousa
Centro ALGORITMI
University of Minho
Guimaraes, Portugal
tsousa@dei.uminho.pt

Delfim Pedrosa
Centro ALGORITMI
University of Minho
Guimaraes, Portugal
dpedrosa@dei.uminho.pt

Vitor Monteiro
Centro ALGORITMI
University of Minho
Guimaraes, Portugal
vmonteiro@dei.uminho.pt

Joao L. Afonso
Centro ALGORITMI
University of Minho
Guimaraes, Portugal
jla@dei.uminho.pt

***Abstract*—This paper presents an enhanced three-phase shunt active power filter (SAPF) that, besides its inherent functionalities of power quality problems compensation, also allows the interface of a renewable energy source (RES, namely solar photovoltaic – PV panels) and an energy storage system (ESS, namely batteries) through its dc-link. On the power grid-side, a three-phase four-wire voltage-source ac-dc converter is connected with the power grid, operating as an SAPF, whereas the RES-interface and the ESS-interface are made through a three-port multilevel dc-dc converter connected to the dc-link of the SAPF. Besides, to compensate power quality problems related to currents, the SAPF also permits the controllability of the bidirectional power exchanged between the power grid and the dc interfaces, i.e., the RES and the ESS. The operation principle of the whole system, as well as the detailed control algorithms, are described in the paper. A validation was performed through computer simulations, where it is possible to analyze the different operation modes of the enhanced SAPF interfacing a RES and an ESS through the dc-link.**

Keywords— Shunt Active Power Filter, Power Quality, Renewable Energy Source, Energy Storage System.

I. INTRODUCTION

Nowadays, due to the growth in the global demand for electricity, there is an increasing interest in the use of renewable energy sources (RES) to produce electricity [1][2][3]. The introduction of RES is contributing to the reduction of greenhouse gas emissions, as well as to transform the traditional power grid, each more from a centralized generation into a decentralized power grid with distributed resources, allowing consumers to participate actively in the market, consuming and producing energy [1][4]. However, in order to mitigate the intermittency associated with the energy generation from RES, the integration of energy storage systems (ESS) is fundamental [5][6][7]. In [8] is presented a review of ESS to be integrated with RES systems. In [9] is presented a control system to optimize the energy management of a grid connected with PV panels and batteries. The association of RES with ESS will optimize energy management in smart grids and smart homes, as demonstrated in [6], [7], and [10]. The integration of RES with ESS into the power grid is performed through power converters, which typically introduce power quality problems, namely current harmonics and low power factor [2][4]. Moreover, this integration, alongside with the large-scale of non-linear loads connected to the power grid, at industrial or residential levels, will decrease the power quality of the power grid [11]. In the last decades, as a solution to improve the power quality of the power grid, active power filters have been widely used [11]. Focusing on the integration of RES with ESS into the power grid, it requires the use of power converters [12], that typically are performed through independent interfaces (for each interface an ac-dc converter and a dc-dc converter is used). However, to increase the efficiency of the system, a single ac-dc converter has been used for the grid-interface, while the RES and ESS are connected through two independent dc interfaces sharing a common dc-link [13].

In this context, in [14] is analyzed the role of connecting active power filters with RES into the power grid as a solution to improve the power quality of the installation. In [15][16] a three-phase shunt active power filter (SAPF), connected in parallel, integrating RES, is presented. A three-phase SAPF integrating PV panels and batteries (as an energy backup) with a single grid-interface is proposed in [17][18]. However, in both topologies, the battery is connected directly to the dc-link of the SAPF and the interface of the PV panels is a two-level dc-dc converter. A computer simulation of a three-phase SAPF integrating PV panels and batteries with a single grid-interface, i.e. only one ac-dc converter, is proposed in [19][20], however the dc interfaces are formed by two-level dc-dc converters. A similar topology is proposed in [21], however for single-phase installations.

In this context, this paper presents an enhanced three-phase SAPF, which allows the interface of a RES (solar photovoltaic – PV panels) and an ESS (batteries), through a common dc-link, with the power grid using a single converter. This paper is a continuation of the work developed in [23], where new improvements are presented, more specifically the validation of the two interfaces operation individually and simultaneously. Moreover, the presented topology can also operate, at the same time, to compensate the power quality problems of the smart grid related to the currents, namely current harmonics, current imbalances, and low power factor. Fig. 1 shows a block diagram of the three-phase SAPF used to interface PV panels and batteries with the power grid. Thus, the main contributions of the presented three-phase SAPF are: analysis of the three-phase topology integrating RES and ESS; possibility of individual control of the grid-interface, RES-interface, and ESS-interface. Regarding the grid-

interface, it can operate as: (a) an active rectifier (absorbing power to charge the batteries); (b) an inverter (injecting power from the RES or from the ESS into the grid); (c) an SAPF combined or not with the operation as an active rectifier or as an inverter. Concerning the dc interfaces, this topology allows to exchange power directly between the RES and the ESS, operates with three voltage levels (improving the quality of the variables controlled by the converter [24]) and the output variables are controlled with the double of the switching frequency.

The topology of a three-phase SAPF is presented in section II, while section III presents the control algorithm. The operation principle of the proposed system is validated in section IV, and the main conclusions are presented in section V.

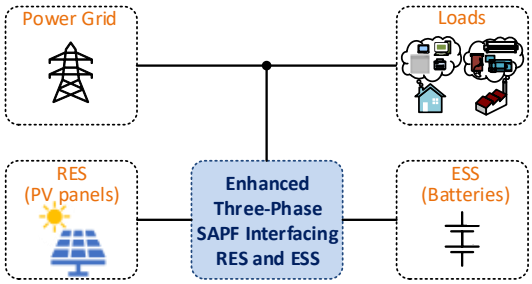

Fig. 1. Block diagram of the proposed enhanced three-phase SAPF used to the interface of a RES (PV panels) and an ESS (batteries) with the power grid.

II. Topology of the Enhanced Three-Phase SAPF

The topology of the enhanced three-phase SAPF integrating a RES and an ESS is shown in Fig. 2 and the main characteristics and parameters are presented in TABLE I. The power grid-side interface is formed by a three-phase ac-dc converter connected in parallel with the power grid for compensating current harmonics, current imbalances, and power factor. The RES-interface and the ESS-interface are made through a multilevel dc-dc converter connected to the dc-link of the three-phase SAPF. The multilevel dc-dc converter can be seen as two dc-dc converters (a unidirectional dc-dc converter used for the RES-interface and a bidirectional dc-dc converter for the ESS-interface).

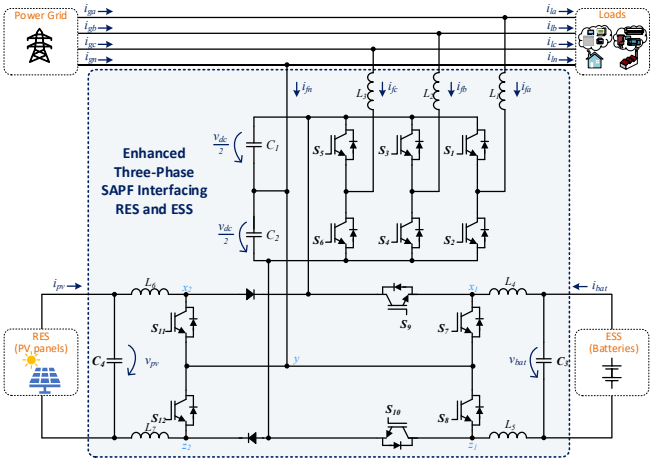

Fig. 2. Topology of the enhanced three phase SAPF used to the interface of a RES (PV panels) and an ESS (batteries) with the power grid.

TABLE I. Characteristics and Parameters of the Enhanced Three-Phase SAPF Integrating a RES and an ESS.

Parameter	Value
RMS power grid voltage (phase-to-phase)	400 V
Nominal power	10 kW
Nominal dc-link voltage	800 V
Nominal batteries voltage	300 V to 500 V
Nominal batteries current	15 A
Nominal PV panels voltage	300 V to 500 V
Nominal PV panels current	15 A
Switching frequency (f_{sw})	20 kHz
Sampling frequency (f_s)	40 kHz
Inductive passive filter (L_1 to L_7)	2.4 mH
Dc-link capacitors (C_1, C_2)	8200 µF
Capacitive passive filter (C_3, C_4)	10 µF

A. Bidirectional ac-dc Converter

For the grid-interface, a three-phase four-wire three-leg voltage-source ac-dc converter is used, using a split dc-link. Depending on the state of the IGBTs, this topology can produce three voltage levels at the phase-to-phase terminals of the converter. Therefore, the ac-dc converter is controlled by current and connected in parallel with the power grid through coupling inductors. In this way, the grid-interface can operate as: (a) active rectifier (power grid providing power to charge the batteries); (b) inverter (power grid receiving power from the PV panels, the batteries, or both interfaces); (c) SAPF combined or not with the operation as an active rectifier or as an inverter (compensating problems related with the currents and the power factor, as well as exchanging power according to the power delivered from the PV panels and the ESS mode).

B. Multilevel dc-dc Converter

As aforementioned, the multilevel dc-dc converter is responsible for the RES-interface and ESS-interface, and it can be seen as two dc-dc converters: a unidirectional dc-dc converter for the RES-interface, whose role is to extract the maximum power delivered by the PV panels; and a bidirectional dc-dc converter for the ESS-interface, responsible for charging/discharging the batteries with a constant current or constant voltage. Traditionally, the dc-dc converters used for these interfaces are two-level topologies. However, it is possible to improve the quality of the variables controlled by the converter using a three-level dc-dc topology [24]. Therefore, the multilevel dc-dc converter is composed of two three-level dc-dc topologies sharing the same dc-link, therefore, according to the state of the IGBTs, each interface can produce three distinct voltage levels at the terminals of the converter (v_{x1y} and v_{yz1} or v_{x2y} and v_{yz2}) [24].

III. Control Algorithm

This section presents the control algorithms for the three-phase SAPF integrating a RES and an ESS. Fig. 3 represents the block diagram of the control algorithm to the system. Initially, the signal variables of the system are acquired with a sampling frequency of 40 kHz through voltage and current sensors, to be applied in a digital signal processor, where the control algorithms are implemented. Thereafter, the obtained output signals are applied to the gate

of the IGBTs (that forms the three-phase SAPF integrating RES and ESS).

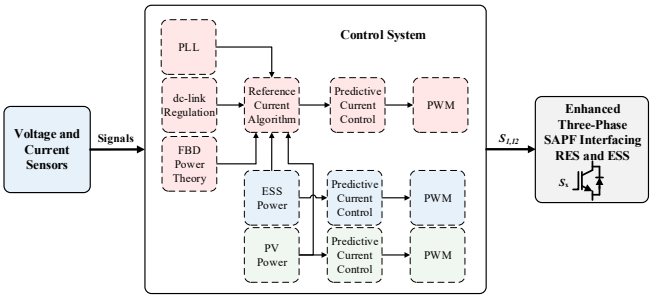

Fig. 3. Block diagram of the control algorithm to the enhanced three-phase SAPF integrating a RES and an ESS.

A. Control Algorithm: Bidirectional ac-dc Converter

Regarding the control algorithm of the grid-interface, it is responsible for controlling the currents produced by the ac-dc converter, compensating the harmonic currents of the load currents, and for the dc-link voltage regulation. The block of the reference currents gives the references that the ac-dc converter must synthesize. For such purpose, a Fryze-Buchholz-Depenbrock (FBD) power theory [25] is used for calculating the reference currents of the grid-interface (i^*_{fx}) for phase x ($x = \{a, b, c\}$), according to:

$$i^*_{fx} = \frac{P_g}{3\,V_{gx}{}^2}\, v_{gx} - i_{lx}\,, x = \{a, b, c\} \tag{1}$$

where P_g is the mean value of the grid power, V_{gx} the RMS grid voltage, v_{gx} the instantaneous power grid voltage and i_{lx} the instantaneous load current. However, in order to avoid the introduction of harmonic components of the power grid voltages (v_{gx}) into the reference currents, a phase-locked loop (PLL) algorithm is used [25]. This strategy uses the power grid voltages (v_{gx}) and generates a unitary signal synchronized with the fundamental component of the grid voltage (v_{pllx}). Moreover, according to the operation modes of the system, the grid power can be fragmented in four parts: (a) the power to regulate the dc-link voltage (P_{dc}); (b) the active power demanded by the loads (P_{load}); (c) the power delivered by the PV panels (P_{pv}); and (d) the power to charge/discharge the batteries (P_{bat}). In this way, the grid power can be established as:

$$P_g = P_{dc} + P_{load} + P_{pv} + P_{bat} \tag{2}$$

As aforementioned, the ac-dc converter is also responsible for the dc-link regulation, in this way the power necessary for regulating the dc-link voltage (P_{dc}) is determined using two proportional-integral (PI) controllers that minimize the error between the dc-link voltages and its references. Therefore, applying (2) in (1), the reference currents of the grid-interface (i^*_{fx}) are calculated according to:

$$i^*_{fx} = \sqrt{2}\ \frac{P_{dc}+P_{load}+P_{pv}+P_{bat}}{3\,V_{gx}}\, v_{pllx} - i_{lx} \tag{3}$$

The currents produced by the ac-dc converter (i_{fx}) are controlled through a current control algorithm that generates a reference voltage (v_{fx}) that the ac-dc converter must produce. The digital implementation of the control algorithm is obtained according to:

$$v_{fx} = v_{gx}[k] - \frac{L}{T_s}\left(i^*_{fx}[k] - i_{fx}[k]\right) \tag{4}$$

Therefore, the signals to be applied to the gate of the IGBTs (that form the ac-dc converter) are obtained using a pulse-width modulation (PWM) technique by comparing the voltage references (v_{fx}) with a triangular carrier.

B. Control Algorithm: Multilevel dc-dc Converter

The multilevel dc-dc converter used for the dc interfaces (PV panels interface and batteries interface) is responsible for controlling the currents produced by the dc interfaces with a constant value. As aforementioned, the multilevel dc-dc converter can be controlled as two dc-dc converters, being used for each dc interface a predictive current control and a modulation with two triangular carriers (shifted 180º). Therefore, with this control strategy, the ripple frequency of the current of the dc interfaces is twice of the switching frequency. Regarding the ESS, when it is controlled to charge the batteries with a constant current, the dc-dc converter operates in buck mode. In this way, based on the representation of the voltages and currents (Fig. 2), the voltages synthesized by the converter are established as (5), where v_{x1y} and v_{yz1} represent the voltages produced by the converter, v_{bat} represents the batteries voltage, v_{L3} represents the voltages in the inductance L_3, and v_{L4} represents the voltages in the inductance L_4.

$$v_{x1y,yz1} = v_{bat} + v_{L_3} + v_{L_4}. \tag{5}$$

As it can be seen, the current in the inductance L_3 is the same as the current in the inductance L_4 (i_{bat}), consequently, (5) can be rewritten as:

$$v_{x1y,yz1} = v_{bat} + (L_3 + L_4)\,\frac{di_{bat}}{dt}. \tag{6}$$

Therefore, by applying the Euler method in (6), the discrete time implementation is obtained according to:

$$v_{x1y,yz1}[k] = v_{bat} + \frac{L_3+L_4}{T_s}\,(i_{bat}{}^*[k] - i_{bat}[k]), \tag{7}$$

where $i_{bat}{}^*[k]$ and $i_{bat}[k]$ represent the reference current at the instant $[k]$ and the current produced by the converter at the time $[k]$, respectively.

The signals to be applied to the gate of the IGBTs S_9 and S_{10} are obtained comparing the voltages synthesized with two triangular carriers (shifted 180º). On the other hand, when the ESS is controlled to discharge the batteries (dc-dc converter operates in boost mode), the voltages synthesized by the converter are established as follows:

$$v_{x1y,yz1}[k] = v_{bat} - \frac{L_3+L_4}{T_s}\,(i_{bat}{}^*[k] - i_{bat}[k]). \tag{8}$$

The gate signals for the IGBTs S_7 and S_8 are obtained comparing the voltages that the converter must produce with two triangular carriers (shifted 180º). Regarding the control of the RES-interface, it is responsible for extracting the maximum power delivered by the PV panels into the dc-link. In this way, by applying the same model for the RES control, the voltages that the converter must produce can be established as follows:

$$v_{x2y,yz2}[k] = v_{pv} - \frac{L_6 + L_7}{T_s}\,(i_{pv}^{*}[k] - i_{pv}[k]), \quad (9)$$

where v_{x2y} and v_{yz2} represent the voltages produced by the converter, v_{pv} represents the voltage in the PV panels, and $i_{pv}^{*}[k]$ and $i_{pv}[k]$ represent the reference current at the instant $[k]$ and the current produced by the converter at the time $[k]$, respectively. Therefore, to obtain the gate signals for S_{11} and S_{12}, the obtained voltages (v_{x2y} and v_{yz2}) are compared with two triangular carriers (shifted 180º).

IV. Validation of the Operation Principle of the Topology

This section presents the validation of the three-phase SAPF integrating a RES and an ESS and its control algorithms, which were obtained through computer simulations using the software PSIM. The simulation results are divided in three subsections: (a) SAPF operating individually; (b) Multilevel dc-dc converter operating individually; (c) SAPF combined with the multilevel dc-dc converter.

A. Shunt Active Power Filter Operating Individually

This section presents the simulation results of the three-phase SAPF operating individually with different types of loads. The SAPF is operating with a non-linear load that consists of a three-phase diode rectifier with an output capacitive filter and a resistive load, and with input inductors. In order to validate the SAPF operating to compensate imbalanced currents, imbalance linear loads (resistive-inductive loads) were connected. Additionally, in phase *a*, it was also connected a diode rectifier with an output resistive-inductive load and input inductor. Fig. 4 presents the simulation results of this operation mode. As it can be seen, with the SAPF operation the grid currents are sinusoidal, balanced and in phase with the respective grid voltage. The total harmonic distortion is reduced from 27% to 5%. The compensation current produced by the SAPF follows its reference and regardless of the SAPF operation, the dc-link voltages are set to the established reference value of 400 V.

To analyze the dynamic response of the SAPF control, were introduced changes in the connected loads. Fig. 5 shows the SAPF response with load changing. Initially, a three-phase diode rectifier with an output capacitive filter and a resistive load and input inductors were connected to the power grid. Moreover, at the instant 0.3 s the resistive load of the three-phase diode rectifier is changed, and it is connected to each phase a resistive-inductive load. Additionally, a diode rectifier with an output resistive-inductive load and input inductor was connected to the phase *a*. It can be observed, that even during the transient state of the SAPF operation the power grid currents (i_{ga}, i_{gb}, i_{gc}) stay sinusoidal, balanced and in phase with the respective power grid voltage (v_{ga}, v_{gb}, v_{gc}). The neutral current in the power grid (i_{gn}) is reduced to approximately 0 A Additionally, the compensation current produced by the SAPF (i_{fa}) follows the SAPF reference current (i^{*}_{fa}), whereas, due to the load connection, the dc-link voltages decrease. However, the SAPF response is fast and the dc-link voltages (v_{dc1}, v_{dc2}) are reestablished to the reference value. On the other hand, Fig. 6 shows the SAPF response with load disconnection at the instant 0.5 s, where, similarly to the mentioned case, during the transient state of the SAPF operation the power grid currents stay sinusoidal, balanced and in phase with the respective power grid voltage. In this case, the dc-link voltages increase, presenting the natural oscillation (values are reestablished fast to their references).

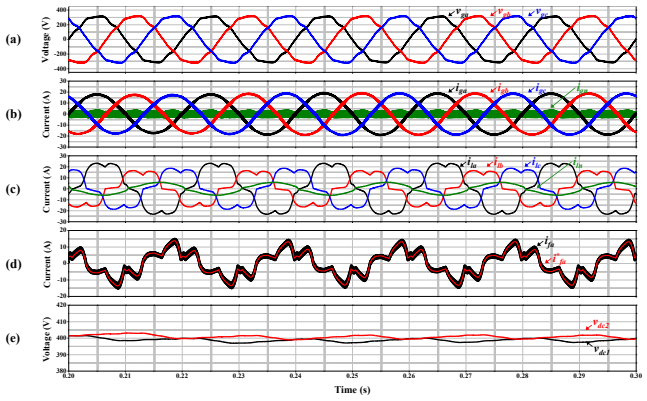

Fig. 4. Simulation results of the system operating as SAPF: (a) Power grid voltages; (b) Power grid currents; (c) Load currents; (d) SAPF reference current and SAPF current for phase *a*; (e) Dc-link voltages.

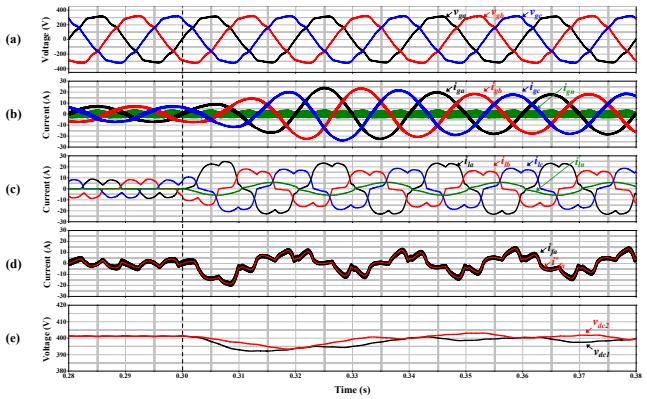

Fig. 5. Simulation results of the system operating as SAPF with load changing: (a) Power grid voltages; (b) Power grid currents; (c) Load currents; (d) SAPF reference current and SAPF current for phase *a*; (e) Dc-link voltages.

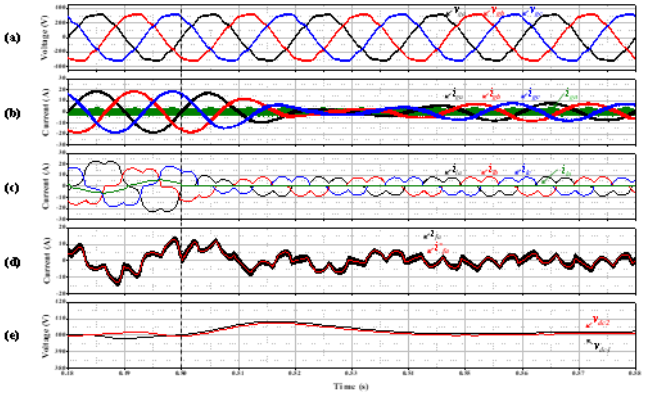

Fig. 6. Simulation results of the system operating as SAPF with load disconnection: (a) Power grid voltages; (b) Power grid currents; (c) Load currents; (d) SAPF reference current and SAPF current for phase *a*; (e) Dc-link voltages.

B. Multilevel dc-dc Converter Operating Individually

This section presents the simulation results of the multilevel dc-dc converter operating individually, transferring energy from the batteries (ESS-interface) to the dc-link. The dc-dc converter is controlled to discharge the batteries with a constant current. Fig. 7 presents the simulation results during the batteries discharging, where, initially, the batteries are discharged with a constant current of 10 A. Afterwards, in order to analyze the dynamic response of the dc-dc converter,

a change in the reference current from 10 A to 15 A was simulated (at the instant 0.3 s). It is noticeable that even with the change in the reference current, the current for batteries discharging (i_{bat}) follows its reference (i^*_{bat}).

Similarly to the previous operation mode, it was simulated a sudden variation of the reference current, where initially the batteries are charging and suddenly change for operating discharging the batteries. Fig. 8 presents the simulation results during the referred scenario. In the first case, the batteries were charged with a constant current of -15 A, whereas in the second case the batteries were discharged with a constant current of 15 A. In both cases, the current produced by the dc-dc converter (i_{bat}) follows its reference (i^*_{bat}).

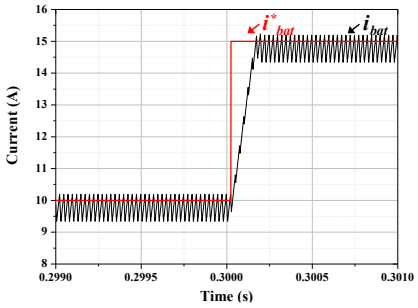

Fig. 7. Simulation results of the multilevel dc-dc converter operating during batteries discharging, when the reference current has a sudden change.

On the other hand, Fig. 9 presents the simulation results of the multilevel dc-dc converter operating transferring energy from the PV panels to the dc-link. As it can be seen, even with changes in the reference current (i^*_{pv}) the current produced by the PV panels (i_{pv}) follows its reference.

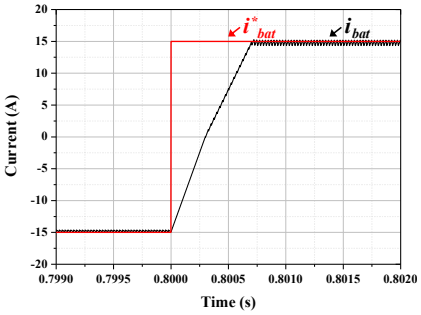

Fig. 8. Simulation results of the multilevel dc-dc converter operating during batteries charging, with a sudden change for operation during batteries discharging.

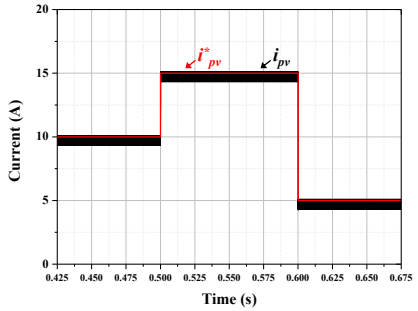

Fig. 9. Simulation results of the multilevel dc-dc converter operating during transference of power from the PV panels to the dc-link.

C. *Shunt Active Power Filter Combined with the Multilevel dc-dc Converter*

This subsection shows the validation of the SAPF combined with the multilevel dc-dc converter. For simplicity, the following simulation results are presented regarding just to one of the power grid phases, in this case phase *a*. Fig. 10 shows the main simulation results of the system. Initially, when the system is not operating, the power grid supplies the loads and the grid current presents high harmonic distortion with a value of 23.2%. At the instant 0.28 s the SAPF starts compensating and the power grid currents become sinusoidal, with an RMS value of 13.6 A, in phase with the power grid voltage. Moreover, it is noticeable that the grid power (P_g) is given by the power requested from the loads (P_{load}). The compensation current (i_{fa}) follows its reference (i^*_{fa}) and the dc-link regulation is set to the reference voltage of 400 V. In the next stage, at the instant 0.36 s, the system is operating as SAPF and transferring energy from the batteries to the power grid. The batteries are discharged with a constant current of 15 A and the grid power (P_g) requested for supplying the loads is given by the difference between the load power (P_{load}) and the power provided by the batteries (P_{bat}). Regarding the grid current, it is sinusoidal and in phase with the grid voltage, with an RMS value of 11.8 A. Therefore, at the instant 0.44 s, the system operates as SAPF combined with the PV panels transferring energy to the power grid. As it turns out, again in this case, the grid current is sinusoidal, with an RMS value of 11.8 A, and in phase with the grid voltage. Concerning the power exchanges, the grid power (P_g) is given by the difference between the power consumed by the loads (P_{load}) and the power extracted from the PV panels (P_{pv}). At the instant 0.52 s, the system is operating as SAPF and charging the batteries with a constant current of 10 A. As it can be seen, the grid current is sinusoidal and in phase, with the grid voltage with a value of 16.4 A RMS given by the current consumed by the loads and the current used to charge the batteries (i_{bat}). Due to the power used to charge the batteries, the dc-link voltages (v_{dc1}, v_{dc2}) decrease up to 390 V. Thereafter, at the instant 0.6 s, the system is operating as SAPF and transferring power from the PV panels and batteries into the power grid. The grid power (P_g) is given by the difference between the load power (P_{load}) and the PV panels power (P_{pv}) and the power from the batteries (P_{bat}). It is noticeable that the grid current is sinusoidal, with an RMS value of 8.3 A, and in phase with the power grid voltage. The batteries were discharged with a constant current of 15 A, whereas the current of the PV panels was controlled to a constant value of 15 A. In the last stage, at the instant 0.68 s, the system is operating as SAPF, transferring energy from the PV panels to the power grid and charging the batteries. The currents of the dc interfaces were controlled to a constant current of 15 A. The grid power (P_g) is given by the difference between the sum of the load power (P_{load}) and the batteries (P_{bat}) with the PV panels power (P_{pv}). During this operation mode, the grid current (i_{ga}) is sinusoidal, with an RMS value of 7.3 A, and in phase with the power grid voltage (v_{ga}). Similarly, the SAPF operation combined with the charging batteries mode, the dc-link voltages (v_{dc1}, v_{dc2}) decrease up to 390 V, due to the power used to charge the batteries.

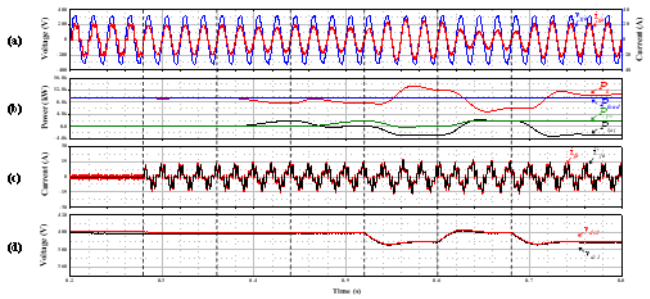

Fig. 10. Simulation results of the three-phase SAPF combined with the multilevel dc-dc converter.

V. Conclusions

This paper presents an enhanced three-phase shunt active power filter (SAPF) interfacing PV panels and batteries through its dc-link. The enhanced three-phase SAPF operates to control the power exchange between the power grid and the dc interfaces, and, at the same time, to compensate the power quality problems related to the currents. On the other hand, the three-port multilevel dc-dc converter is responsible for controlling the power extraction from the PV panels, using a MPPT algorithm, and for charging/discharging the batteries with a constant current. Throughout the paper, the operation principle of the proposed system, as well as the detailed control algorithms, were validated through computer simulations. The simulation results obtained show that for all the operation modes the currents in the grid-interface are kept sinusoidal, balanced and in phase with the respective voltage. Regarding to the currents produced by the dc-dc converters in the dc interfaces are controlled and kept with constant values.

Acknowledgment

This work has been supported by FCT – Fundação para a Ciência e Tecnologia within the R&D Units Project Scope: UIDB/00319/2020. This work has been supported by the FCT Project newERA4GRIDs PTDC/EEI-EEE/30283/2017. Tiago J. C. Sousa is supported by the doctoral scholarship SFRH/BD/134353/2017 granted by FCT.

References

[1] X. Yu, C. Cecati, T. Dillon and M. G. Simões, "The New Frontier of Smart Grids," *IEEE Industrial Electronics Magazine*, vol. 5, no. 3, pp. 49-63, 2011.

[2] T. Strasser *et al*., "A Review of Architectures and Concepts for Intelligence in Future Electric Energy Systems," *IEEE Transactions on Industrial Electronics,* vol. 62, no. 4, pp. 2424-2438, 2015.

[3] H. Kanchev, D. Lu, F. Colas, V. Lazarov and B. Francois, "Energy Management and Operational Planning of a Microgrid with a PV-Based Active Generator for Smart Grid Applications," *IEEE Transactions on Industrial Electronics*, vol. 58, no. 10, pp. 4583-4592, 2011.

[4] Golovanov, N., Lazaroiu, G. C., Roscia, M., & Zaninelli, D., "Power quality assessment in small scale renewable energy sources supplying distribution systems." Energies 6.2 (2013): 634-645.

[5] S. Vazquez, S. M. Lukic, E. Galvan, L. G. Franquelo and J. M. Carrasco, "Energy Storage Systems for Transport and Grid Applications," *IEEE Transactions on Industrial Electronics,* vol. 57, no. 12, pp. 3881-3895, 2010.

[6] Suberu, M. Y., Mustafa, M. W. and Bashir, N. "Energy storage systems for renewable energy power sector integration and mitigation of intermittency." Renewable and Sustainable Energy Reviews 35 (2014): 499-514.

[7] B. P. Roberts and C. Sandberg, "The Role of Energy Storage in Development of Smart Grids," *Proceedings of the IEEE*, vol. 99, no. 6, pp. 1139-1144, 2011.

[8] Carrasco, J. M., Franquelo, L. G., Bialasiewicz, J. T., Galván, E., PortilloGuisado, R. C., Prats, M. M., Moreno-Alfonso, N, "Power-Electronic Systems for the Grid Integration of Renewable Energy Sources: A Survey," *IEEE Transactions on Industrial Electronics*, vol. 53, no. 4, pp. 1002-1016, 2006.

[9] Y. Riffonneau, S. Bacha, F. Barruel and S. Ploix, "Optimal Power Flow Management for Grid Connected PV Systems with Batteries," *IEEE Transactions on Sustainable Energy*, vol. 2, no. 3, pp. 309-320, 2011.

[10] M. Liserre, T. Sauter and J. Y. Hung, "Future Energy Systems: Integrating Renewable Energy Sources into the Smart Power Grid Through Industrial Electronics," *IEEE Industrial Electronics Magazine*, vol. 4, no. 1, pp. 18-37, 2010.

[11] Afonso, João L., J. G. Pinto, and Henrique Gonçalves, "Active power conditioners to mitigate power quality problems in industrial facilities." Power Quality Issues. IntechOpen, 2013.

[12] Vítor Monteiro, Tiago J. C. Sousa, Delfim Pedrosa, Sérgio Coelho, João L. Afonso, "A Three-Level dc-dc Converter for Bipolar dc Power Grids: Analysis and Experimental Validation", IEEE IECON 2020 - Industrial Electronics Conference, Singapore (virtual conference), Oct. 2020, pp.3761-3766.

[13] Monteiro, Vítor, J. Gabriel Pinto, and João L. Afonso, "Experimental validation of a three-port integrated topology to interface electric vehicles and renewables with the electrical grid." IEEE Transactions on Industrial Informatics 14.6 (2018): 2364-2374.

[14] Khadem, Shafiuzzaman Khan, Malabika Basu, and Michael Conlon, "Power quality in grid connected renewable energy systems: Role of custom power devices." (2010).

[15] J. G. Pinto, R. Pregitzer, Luís F. C. Monteiro, João L. Afonso, "3-Phase 4-Wire Shunt Active Power Filter with Renewable Energy Interface," International Conference on Renewable Energies and Power Quality, 28-30 March 2017.

[16] Singh, M., Khadkikar, V., Chandra, A., & Varma, R. K, "Grid interconnection of renewable energy sources at the distribution level with power-quality improvement features." IEEE transactions on power delivery 26.1 (2010): 307-315.

[17] Senguttuvan, S., and M. Vijayakumar, "Solar photovoltaic system interfaced shunt active power filter for enhancement of power quality in three-phase distribution system." Journal of Circuits, Systems and Computers 27.11 (2018): 1850166.

[18] Mousazadeh, S. Y., Savaghebi, M., Beirami, A., Jalilian, A., Guerrero, J. M., & Li, C, "Control of a multi-functional inverter for grid integration of PV and battery energy storage system." 2015 IEEE 10th International Symposium on Diagnostics for Electrical Machines, Power Electronics and Drives (SDEMPED).

[19] Rahmani, S., Hamadi, A., Al-Haddad, K., & Kanaan, H. Y, "A multifunctional power flow controller for photovoltaic generation systems with compliance to power quality standards." IECON 2012-38th Annual Conference on IEEE Industrial Electronics Society.

[20] Ding, F., Li, P., Huang, B., Gao, F., Ding, C., & Wang, C. "Modeling and simulation of grid-connected hybrid photovoltaic/battery distributed generation system." CICED 2010 Proceedings. IEEE, 2010.

[21] Akkala, K., Faranda, R., Sodini, P., & Hafezi, H, "Distributed storage system with solar photovoltaic energy source." IEEE International Conference on Environment and Electrical Engineering and 2019 IEEE Industrial and Commercial Power Systems Europe. IEEE, 2019.

[22] Ana M. C. Rodrigues, Cátia F. Oliveira, Tiago J. C. Sousa, Luís Machado, João L. Afonso, Vítor Monteiro, "Unified Three-Port Topology Integrating a Renewable and an Energy Storage System with the Grid-Interface Operating as Active Power Filter", IEEE CPE-POWERENG 2020 – International Conference on Compatibility, Power Electronics and Power Engineering, Setúbal, Portugal, Jul. 2020, pp.502-507.

[23] V. Monteiro, T. J. C. Sousa, M. J. Sepulveda, C. Couto, A. Lima and J. L. Afonso, "A Proposed Bidirectional Three-Level dc-dc Power Converter for Applications in Smart Grids: An Experimental Validation," 2019 International Conference on Smart Energy Systems and Technologies (SEST), 2019, pp. 1-6.

[24] Staudt, Volker, "Fryze-Buchholz-Depenbrock: A time-domain power theory.", 2008 International School on Nonsinusoidal Currents and Compensation. IEEE, 2008.

[25] L. G. B. Rolim, D. R. Da Costa, M. Aredes, "Analysis and software implementation of a robust synchronizing PLL circuit based on the pq theory," IEEE Trans. Ind. Electron., vol.53, no.6, pp.1919-1926, 2006.